PCCP

Accepted Manuscript

ROYAL SOCIETY OF CHEMISTRY

www.rsc.org/pccp

Theoretical investigation on carbon nucleation on nickel carbides at initial stages of single-walled carbon nanotube formations

Zhimin Yang,[†] Qiang Wang,[†] Xiaoye Shan,[†] Shuo-Wang Yang,[‡] and Hongjun Zhu,*[†]*

[†] Department of Applied Chemistry, College of Science, Nanjing Tech University, Nanjing 211816, P. R. China

[‡] Institute of High Performance Computing, 1 Fusionopolis Way, 16-16 Connexis, Singapore 138632

*Corresponding E-mail: wangqiang@njtech.edu.cn; zhuhj@njtech.edu.cn

Tel. / Fax: +86-25-83172358

Abstract

It is a long-standing controversy whether metal carbide clusters do exist during the nucleation and growth process of single-walled carbon nanotubes (SWCNTs). In the current work, we are trying to elucidate the carbon nucleation on nickel carbides during the initial stages based on density functional theory calculated the formation energy, and chemical potential for a series of $Ni_{55}C_n$ carbides (*n* is the number of carbon atoms dissolved in Ni_{55} cluster). It is found that the formation energies of the $Ni_{55}C_n$ carbides decrease gradually with increasing of dissolved carbon atomic numbers, meaning the $Ni_{55}C_n$ carbides are thermodynamically stable. Meanwhile, the calculated chemical potentials indicate that not only nickel carbides are preferentially formed during the initial stage of the SWCNT nucleation, but also saturated nickel carbides may be able to exist during nucleation and growth process of SWCNTs. In addition, the nickel carbides have a high selectivity for the formation of carbon pentagon and carbon structures with pentagon-incorporated end-edge according to the adsorption energies. All of these findings provide opportunities in controlling growth of the SWCNT.

KEYWORDS: nickel carbide, formation energy, chemical potential, single-walled carbon nanotube nucleation, DFT calculations

Table of content

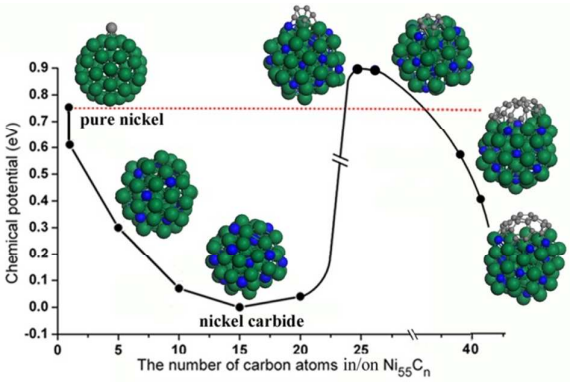

A first-principles study shows metal carbide clusters do exist during initial stage of single-walled carbon nanotube nucleation.

Introduction

Single-walled carbon nanotubes (SWCNTs) have been attracting a lot of interest in the past decades due to their unique physical and electronic properties[1, 2] which strongly depend on their diameter, length, and chirality.[3, 4] Control growth of SWCNTs with specific diameter, length and chirality is essential for their nanoscale assembly and technological applications.[1, 2] It is widely accepted that carbon (C) atoms adsorb on metal clusters before diffuse/penetrate into these clusters at initial steps of the SWCNT growth. Those C atoms on/within metal/metal-carbide clusters further incorporate into carbon caps, and eventually grow into SWCNTs on metal/metal-carbide clusters.[5-7] It is noted that metal or metal-carbide clusters play important roles in decomposition of carbon precursors, healing defects of growing nanotubes, and keeping critical carbon density for nanotube growth.[8-11] Experimental and theoretical studies have shown that the sizes, morphology, and composition of metal/metal-carbide clusters determine the diameter, length, and chirality of SWCNTs.[4, 12-15] However, it is still a controversy whether metal carbide clusters do exist during the nucleation and growth process of SWCNTs.[16-21]

Recent experimental studies have shown the existence of Ni_3C[16, 17] and Fe_3C[18, 19] carbide clusters prior to initial nucleation or the whole growth processes of SWCNTs; It has been reported carbon atoms may dissolve in crystalline metal clusters and

supersaturated carbon in the surface area precipitates as graphene. The theoretical studies also indicate the carbon diffusion from on-surface site to octahedral subsurface site is thermodynamically and kinetically feasible. The activation barriers of carbon diffusion strongly depend on the size of unit-cell/cluster and on the surface coverage.[22-26] Subsurface and bulk carbons are often proposed as intermediates in the formation of carbon nanotubes and graphene. Recently, Ding *et al*. proposed that the higher concentrations of carbon in metal clusters are prerequisite for forming the initial small carbon island, and then it decreases as the islands grow in size.[27] Borjesson *et al*. evidenced that dissolved C atoms would be drained from the Ni carbide clusters by the CNTs sunk in carbide clusters.[28] Page *et al.* also assumed that carbon would be drawn out from metal carbide clusters when surface structural C atoms began to nucleate, which leads carbide clusters with higher content to quickly decrease their carbon concentration.[29] On the other hand, both pure Ni[20] and Fe[21] catalyst clusters have also been observed in growth process of SWCNTs. Meanwhile, theoretical studies also suggested that a carbide phase is not essential prerequisite for the SWCNT nucleation in Fe and Ni cases.[30, 31]

In our recent study, we have studied the adsorption of carbon atom on various Ni clusters. The results show that carbon atom adsorbed on-surface site can migrate into the octahedral subsurface site with low activation barrier about 0.26 eV. In order to

further address whether metal carbide clusters can be formed at initial stage of SWCNT nucleation, in current work, we extended our study to C atom nucleation on a series of $Ni_{55}C_n$ carbides and carbon rings and caps adsorbed on $Ni_{55}C_{20}$ carbide based on calculated formation energies and chemical potentials. Here, *n* is the number of carbon atoms dissolved in Ni_{55} cluster and n = 5, 10, 15, and 20, respectively. These results and conclusions should be helpful in deeply understanding of the SWCNT nucleation and growth.

2. Computational Methodology and models

All spin polarized density functional theory calculations were performed with the Vienna *Ab initio* simulation package (VASP)[32]. The exchange correlation function were treated using the generalized gradient approximation (GGA) formulated by the Perdew-Burke-Ernzerhof (PBE)[33]. The interaction between an atomic core and electrons were described by the projector augmented wave method.[34, 35] The plane-wave basis set energy cutoff was set to 400 eV. We used a 1×1×1 k-point mesh for the reciprocal space integration for all the calculated systems with a discrete character. The periodic boundary conditions were implemented with at least 1 nm vacuum to preclude interaction between a cluster and its image, the simulation boxes were 22×22×22 Å for different calculated systems. All of the structures were fully relaxed

to optimize without any restriction. The global transferred charge was calculated by the atomic Bader charge analysis [36, 37].

The formation energy (E_f) per atom of the $Ni_{55}C_n$ carbide clusters was defined according to Eq. 1 as follows:

$$E_f = \frac{E_{Ni_{55}C_n} - E_{Ni_{55}} - nE_C}{n+55} \quad (1)$$

The chemical potential (μ) of the carbon in/on $Ni_{55}C_n$ carbides, which is the energy in need of adding one extra carbon atom into $Ni_{55}C_n$ carbides or growing carbon structures, was defined as

$$\mu = \frac{E_{Ni_{55}C_n} - E_{Ni_{55}}}{n} - \mu_C \quad (2)$$

where $E_{Ni_{55}C_n}$ and $E_{Ni_{55}}$ are the total energies of optimized geometry complexes with and without C atoms, E_C is the energy of a free carbon at its ground state, respectively. Here, n is the number of carbon atoms in/on each $Ni_{55}C_n$ carbides. The reference chemical potential, μ_C, is the chemical potential of a free carbon atom at its ground state, 7.70 eV.[38] The chemical potential has previously been applied in SWCNT nucleation and growth studies.[39]

Ni_{55} and $Ni_{55}C_n$ Models: Pure Ni_{55} and $Ni_{55}C_n$ (n=5, 10, 15, and 20) carbide clusters were modelled in Fig. 1 and 2. The Ni_{55} cluster was chosen because its diameter (about 1 nm) is consistent with mostly synthesized SWCNT diameter distributions. Both experimental and theoretical studies have shown that the diameter ratio between a catalyst cluster and its corresponding SWCNT is around 1.1–1.6.[39, 40]

In addition, the Ni_{55} cluster has been observed in SWCNT growth experiments,[40, 41] and adopted in our previous studies of SWCNT growth as well.[42-44] The pure Ni_{55} cluster with a symmetrical icosahedral structure is a local energy minimum in its size range.[35] As illustrated in Fig. 1, the Ni_{55} has one atom at the centre, 12 atoms locating at sublayer, and 42 atoms situating on surface layer of icosahedral cluster. Thus, there are 20 octahedral subsurface sites between sublayer and surface layer of the icosahedral Ni_{55} cluster. The 20 octahedral subsurface sites distribute in top (5 sites), middle-1 (5 sites), middle-2 (5 sites), and bottom (5 sites) of the Ni_{55} cluster, respectively.

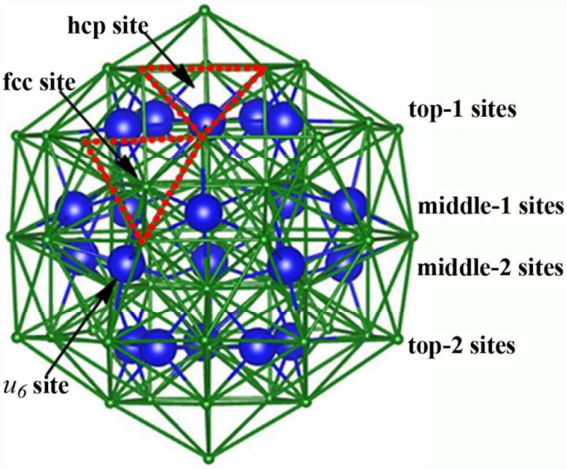

Fig. 1. Schematic optimized structure of Ni_{55} has a high symmetrical icosahedral geometry. Surface adsorption and subsurface dissolved sites are depicted on the model. Green spheres represent Ni atoms. Blue spheres represent 20 subsurface sites.

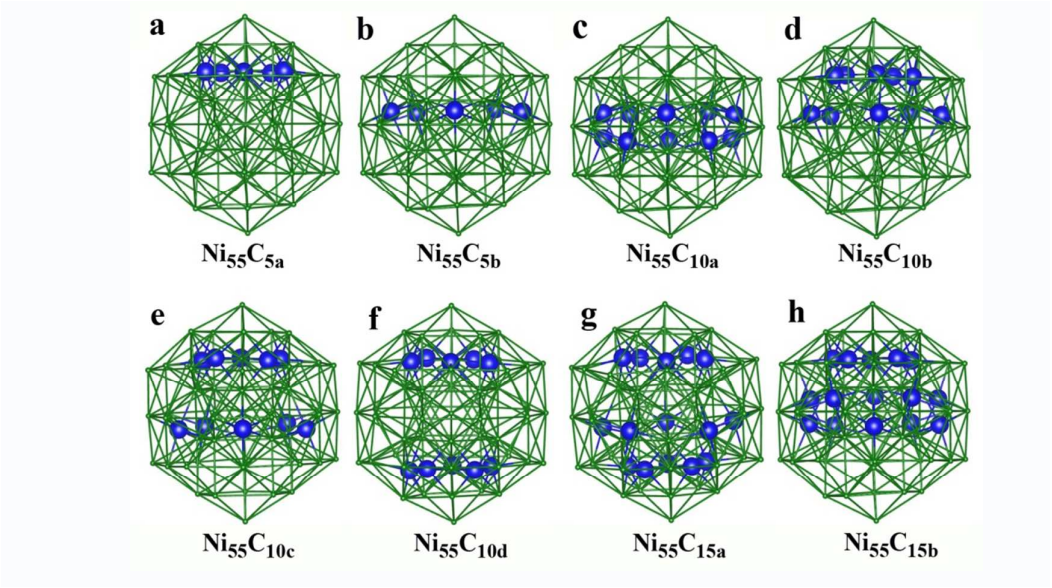

Fig. 2. Schematic initial configurations of $Ni_{55}C_n$ carbides (n=5, 10, 15, and 20). The high symmetrical icosahedral geometries are adopted as initial structures for $Ni_{55}C_n$ carbides. The simulated structures are fully relaxed without any constraint, thus these carbide clusters would deviate from their initial configurations after optimization (see Fig. 3). Green and blue spheres represent Ni and C atoms, respectively.

Since $Ni_{55}C_n$ carbide clusters have many complicated geometric configurations with different distribution pattern and different number of carbon atoms positioned into 20 subsurface sites, it is impractical to optimize all of them. Here, based on the C atomic number we are considering four types of C representative initial ordering configurations. They are (a) two $Ni_{55}C_5$ configurations: five C atoms are positioned into five subsurface sites in the top-1 (denoted as $Ni_{55}C_{5a}$ in Fig. 2a) or middle-1 (denoted as $Ni_{55}C_{5b}$ in Fig. 2b) of the Ni_{55} cluster, respectively; (b) four $Ni_{55}C_{10}$ configurations: ten C atoms were equally positioned into five subsurface sites in the middle-1 and middle-2 (denoted as $Ni_{55}C_{10a}$ in Fig. 2c), top-1 and middle-1 (denoted as $Ni_{55}C_{10b}$ in Fig. 2d), top-1 and middle-2 (denoted as $Ni_{55}C_{10c}$ in Fig. 2e), and two end tops (denoted as $Ni_{55}C_{10d}$ in Fig. 2f) of the Ni_{55} cluster, respectively; (c) two

$Ni_{55}C_{15}$ configurations: 15 C atoms were positioned equally in five subsurface sites in the two end tops, and middle-2 (denoted as $Ni_{55}C_{15a}$ in Fig. 2h) and top-1, middle-1 and middle-2 (denoted as $Ni_{55}C_{15b}$ in Fig. 2h) of the Ni_{55} cluster, respectively; (d) one $Ni_{55}C_{20}$ configuration: 20 subsurface subsurface sites of the Ni_{55} were fully filled up with 20 C atoms, forming a saturated $Ni_{55}C_{20}$ complex (see Fig. 1). To simplify the notation, we would use the number of carbon atoms in the $Ni_{55}C_n$ carbide to indicate the fraction of the subsurface sites occupied by carbon atoms in subsurface layer of Ni_{55}.

3. Results and Discussion

3.1 $Ni_{55}C_n$ (n=5, 10, 15, and 20) carbide clusters

Table 1. Total energy E_t (eV), formation energy E_f (eV/atom), and chemical potential μ (eV) of the $Ni_{55}C_n$ (n=5, 10, 15, and 20) carbides.

Cluster	C%	E_t (eV)	E_f (eV/atom)	μ (eV)
Ni_{55}	0	-255.75	/	/
$Ni_{55}C_{fcc}$	2	-263.96	-0.12	0.76
$Ni_{55}C_{hcp}$	2	-264.12	-0.13	0.61
$Ni_{55}C_{5a}$	9	-297.74	-0.59	0.58
$Ni_{55}C_{5b}$	9	-299.15	-0.62	0.30
$Ni_{55}C_{10a}$	18	-343.86	-1.16	0.17
$Ni_{55}C_{10b}$	18	-344.45	-1.17	0.11
$Ni_{55}C_{10c}$	18	-344.84	-1.17	0.07
$Ni_{55}C_{10d}$	18	-346.08	-1.19	-0.05
$Ni_{55}C_{15a}$	27	-388.92	-1.63	0.10
$Ni_{55}C_{15b}$	27	-390.39	-1.65	0.00
$Ni_{55}C_{20}$	36	-434.59	-2.04	0.04

The optimized structures of the $Ni_{55}C_n$ (n=5, 10, 15, and 20) carbides are depicted in Fig. 3 and detailed results including total energy E_t, formation energy E_f, and chemical potential μ (eV) of the $Ni_{55}C_n$ (n=5, 10, 15, and 20) carbides are given in Table 1. The geometric structure parameters of all the optimized $Ni_{55}C_n$ carbides are given in Table 1s in Supporting Information (SI). The results listed in Table 1

show the total energies variation among carbide isomers is 1.41 eV for $Ni_{55}C_{5a}$ and $Ni_{55}C_{5b}$, 2.22 eV for $Ni_{55}C_{10a}$, $Ni_{55}C_{10b}$, $Ni_{55}C_{10b}$, and $Ni_{55}C_{10d}$, and 1.47 eV for $Ni_{55}C_{15a}$ and $Ni_{55}C_{15b}$, respectively. The difference in the total energy can be explained by both the difference of distribution pattern and coordination number of the C atoms in the $Ni_{55}C_n$ carbides as depicted in Fig. 3. Thereby, the total energies of the $Ni_{55}C_n$ carbides depend on the distribution pattern and coordination number of each C atom in the $Ni_{55}C_n$ carbides.

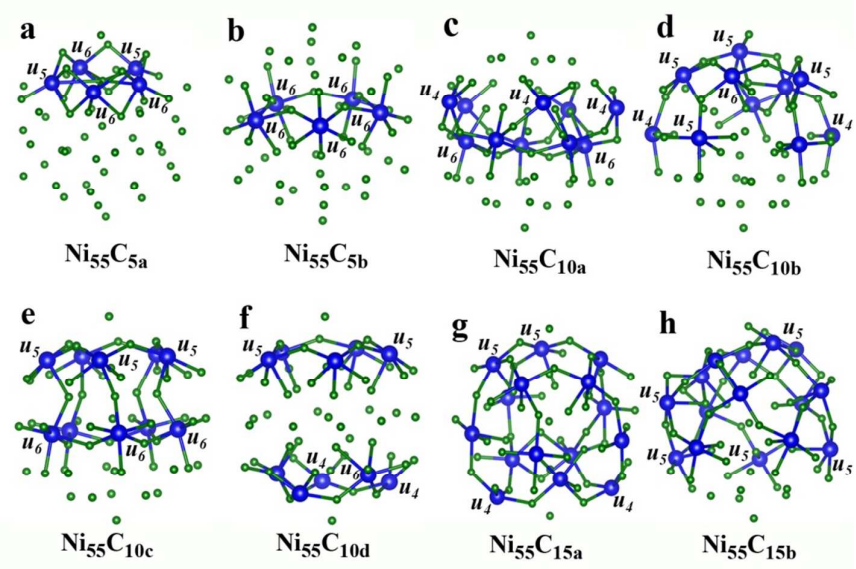

Fig. 3. Optimized structures of the $Ni_{55}C_n$ (n=5, 10, 15, and 20) carbides. Green and blue spheres represent Ni and C atoms, respectively. μ_4, μ_5, and μ_6 denote the C atoms coordinated with four, five, or six Ni atoms, respectively. Detailed structure parameters of all the optimized $Ni_{55}C_n$ carbides are given in Table 1s in SI. The optimized structures correspond to the initial configurations of the $Ni_{55}C_n$ carbides as schematic in Fig. 2.

In addition, all considered $Ni_{55}C_n$ carbides have negative formation energies (see Fig. 4), indicating these $Ni_{55}C_n$ carbides are thermodynamically stable. And these formation energies become more negative gradually with the increase of the C atomic numbers in the $Ni_{55}C_n$ carbides. It suggests C atoms are more inclined to migrate into subsurface sites continuously, leading to more stable $Ni_{55}C_n$ carbides with different concentration. Interestingly, the formation energy differences among carbide isomers (with the same C atomic number n) are only ~ 0.03 eV/atom (see Fig. 4). Considering the sufficiently high nucleation temperature in experiments, such small energy difference suggests various carbide isomers with different distribution patterns and concentration are likely to co-exist during the initial stages of the SWCNT nucleation.

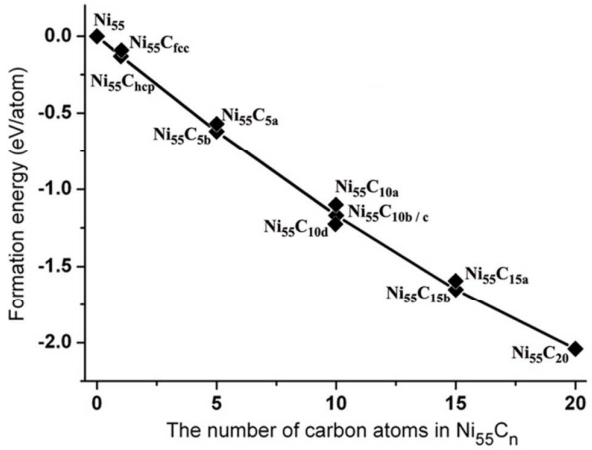

Fig. 4. Formation energies of the $Ni_{55}C_n$ (n=5, 10, 15, and 20) carbides. The number of carbon atom corresponds to the optimized structures of the $Ni_{55}C_n$ carbides as schematically shown in Fig. 3.

At initial stage of the SWCNT nucleation, small carbon species would firstly adsorb on metal cluster surface. The chemical potentials for the first carbon atom on

Ni_{55} surface are 0.76 eV for fcc and 0.61 eV for hcp sites (see Fig. 1 and Table 1), respectively, which higher than chemical potentials of carbon atom resided in subsurface (0.36 eV for μ_5-sub and 0.29 eV for μ_6-sub sites). Note that only the chemical potentials of carbon atom at the fcc and hcp sites are shown on the Fig. 5. In addition, chemical potentials of a C_2 dimer and a C_3 chain adsorbed on the Ni_{55} surface sites are 0.68 and 0.73 eV respectively, which are also higher than that of single carbon in subsurface sites. These values suggest the carbon atom would rather penetrate into the Ni_{55} cluster than stay on the surface. Furthermore, the chemical potentials of $Ni_{55}C_n$ carbides are distinctly lower than that of small carbon species on the Ni_{55} surface (red line in Fig. 5). At the beginning, the chemical potential drops dramatically along with the more and more carbon atoms penetrate into Ni_{55} cluster until it closes to zero for the $Ni_{55}C_{10}$ isomers (see Fig. 5). Subsequently, there is a minor change from $Ni_{55}C_{10}$ to $Ni_{55}C_{20}$, which implies that extra C atoms can continually dissolve into Ni_{55} cluster spontaneously. It is likely that the $Ni_{55}C_n$ carbides with different C concentration can be formed during the initial stage of the SWCNT nucleation.

In our recent study, we have reported that C atom adsorbed on the surface of Ni_{38} and Ni_{55} clusters can migrate into octahedral subsurface sites with a low activation barrier (~0.26 eV).[35] For the periodic slab surface system, Xu and Saeys

reported that C atom diffused into subsurface octahedral sites strongly depend on the size of unit cell and the surface coverage.[25] The typical activation barriers were less than 110 KJ/mol for the moderate to high surface coverage. In addition, Carbon diffusion from subsurface sites to Ni bulk is also thermodynamically and kinetically feasible if subsurface sites are occupied more than 50%. Compared with their activation barriers, C atom diffusion in cluster system (such as Ni_{38} and Ni_{55}) have lower activation barriers, Thus it is expected the C diffusion in cluster system should be easier than in the periodic slab and bulk systems. Recently, Vines *ea al* also reported that the C atom diffusion from Pb cluster surface into tetrahedral subsurface sites is almost non-activation-barriers.[45] They proposed this is due to the high mobility of low-coordinated atoms at cluster edges. These results indicate it is thermodynamically and kinetically feasible for C atom adsorbed on cluster surface diffusion into the subsurface sites. In current work, the results of formation energy and chemical potential further demonstrate the $Ni_{55}C_n$ carbides with different C concentration would be formed during the initial stage of the SWCNT nucleation, and further support the previous speculations the C atoms may enter the metal nanoclusters during CNT growth.

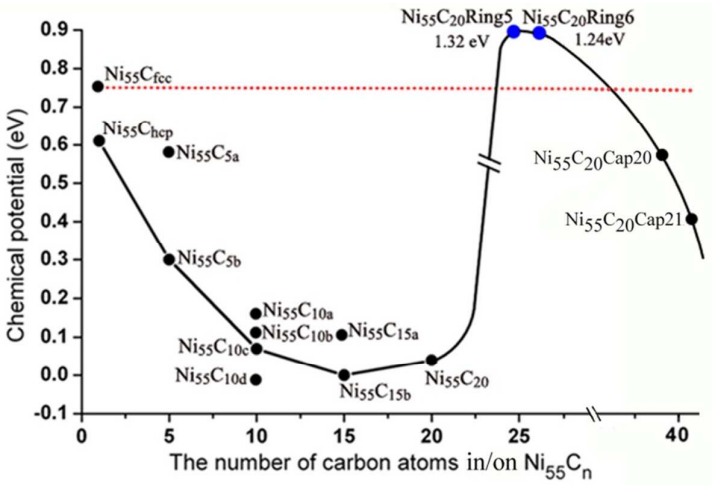

Fig. 5. Chemical potentials (μ) of the $Ni_{55}C_n$ (n=5, 10, 15, and 20) carbides and small carbon rings and caps on the $Ni_{55}C_{20}$ carbides. μ is the energy required to add one extra carbon atom on/in the $Ni_{55}C_n$ carbides. The red line indicates the μ of the C on the fcc sites of the Ni_{55} cluster. The number of carbon atoms corresponds to the optimized structures of the $Ni_{55}C_n$ carbides as schematic in Fig. 3.

3.2 Carbon rings and caps on $Ni_{55}C_{20}$ carbide

In order to investigate the roles played by the metal carbide clusters at the initial stage of the SWCNT nucleation, we further examined the interaction of the $Ni_{55}C_{20}$ carbide with various growing carbon structures. On the basis of the root growth hypothesis, following the formation of various carbon chains and rings, graphitic fragment would evolve into complete carbon caps on catalyst cluster surface. The two pathways, (a)→(c) (the top row of Fig. 6) and (d)→(f) (the bottom row of Fig. 6), illustrate the formation of two typical armchair (5,5) and zigzag (9,0) caps (see to Fig. 6 c and f). It is should be noted that the models shown in Fig. 6 are only representative carbon fragments for the formation of (5,5) and (9,0) chiral caps. The intermediate

fragments were selected because they are the experimentally observed dominating C precursor such as Cap21[46, 47] and adopted in our previous studies[43, 44]. The actual growth process may be less orderly, with numerous polyyne chains and incomplete carbon rings, which have been shown in recent molecular simulations.[48]

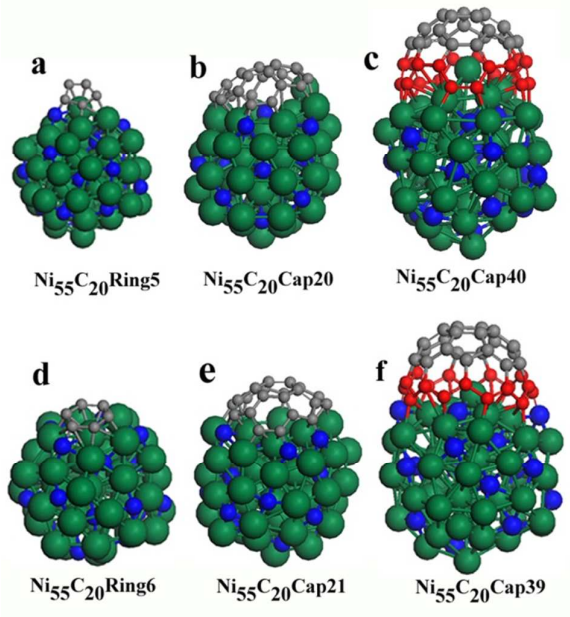

Fig. 6. Optimized structures (side view) of carbon rings and caps attached on the $Ni_{55}C_{20}$ carbides. Grey and blue spheres represent surface-C and subsurface-C, green spheres represent Ni atoms, and end-edges of armchair (5,5) and zigzag (9,0) caps are highlighted as red spheres, respectively.

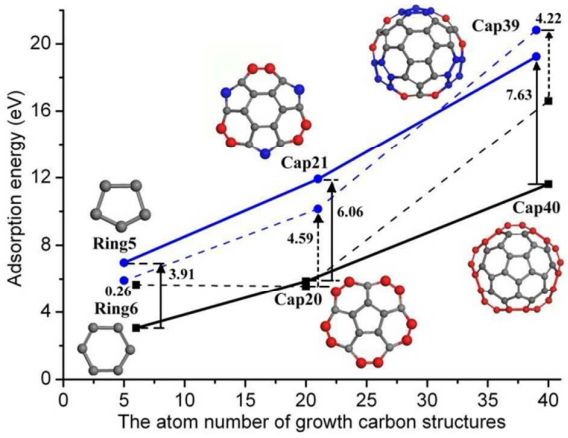

Fig. 7. Adsorption energies of carbon rings and caps supported on the $Ni_{55}C_{20}$ carbide (solid lines) and pure Ni_{55} (dash lines) clusters. The inserted figures show the geometric structures (top view) of the corresponding carbon rings and caps in Fig. 6. The end-edge atoms are highlighted as blue balls (pentagon) and red balls (hexagon). The number of carbon atoms corresponds to the optimized structures as schematic in Fig. 6.

Fig. 7 depicts adsorption energies of carbon rings and caps supported on the $Ni_{55}C_{20}$ carbide and pure Ni_{55} clusters. The geometric structures of corresponding carbon rings and caps are inserted in the graph of Fig.7. The results show that the adsorption energies of carbon rings and caps depend on their unique topological structures. The carbon pentagon and the end-edges with three pentagons-incorporated have significantly higher adsorption energies, while the carbon hexagon and hexagon-only end-edges have notably lower adsorption energies. As shown in Fig. 7, the adsorption energy of five-membered carbon ring on the $Ni_{55}C_{20}$ carbide is 6.96 eV, which is 3.91 eV higher than that of six-membered carbon ring, which suggest that the carbon Ring5 may be preferentially formed over Ring6 on the $Ni_{55}C_{20}$ carbide. This result is consistent with previous first-principle calculations[49] and molecular dynamic simulations[29, 31, 50]. Irle et al. recently reported that, at 1400K, five-membered rings, instead of six- and seven-membered rings, were preferentially formed during the SWCNT nucleation process. Furthermore, they demonstrated the populations of five-,

six- and seven-membered rings exhibited a distinct dependence on the temperature and carbon concentration of Ni_xC_y nanoparticles. [29, 31, 50]

The adsorption energies of Cap21 and cap39 on the $Ni_{55}C_{20}$ carbide are 11.92 and 19.24 eV, which are about 103% and 66% higher than that of the Cap20 and Cap40, 5.86 and 11.61 eV, respectively. The difference in the adsorption energy is attributed to unique end-edge topological structures of various carbon caps. Every edge atom of a pentagon has two dangling bonds, while every edge C atom of a hexagon has one dangling bond. Although Cap21 and Cap39 have 9 edge C atoms apiece, less than 10 edge C atoms of the Cap20 and Cap40, the end-edges of Cap21 and Cap39 actually possess the 12 effective dangling bonds to interact with $Ni_{55}C_{20}$ cluster, while the end-edges of Cap20 and Cap40 have only 10 dangling bonds to interact with $Ni_{55}C_{20}$ cluster. Thereby, the adsorption energies of Cap21 and 39 are significantly stronger than that of the Cap20 and Cap40, which is consistent with a recent study of ground-state structures of C clusters supported on Ni(111), Cu(111), Rh(111), and Ru(0001) surfaces[46].

In addition, compared with the same carbon systems adsorbed on pure Ni_{55} cluster, the results of adsorption energies show the same trend of these carbon systems on the $Ni_{55}C_{20}$ carbide and pure Ni_{55} clusters as shown in Fig. 7 (solid and dash lines) and Table S2 in the SI. Interestingly, the adsorption energy differences of five- and

six-membered carbon rings on $Ni_{55}C_{20}$ carbide and pure Ni_{55} clusters are enlarged from 0.26 to 3.91 eV. Furthermore, for the carbon caps with pentagon-incorporated and hexagon-only end-edges, the adsorption energy differences are also enlarged from 4.59 to 6.06 eV for Cap21 and Cap20, and from 4.22 to 7.63 eV for Cap39 and cap40, respectively. These results imply that the $Ni_{55}C_{20}$ carbide has a better selectivity for the pentagon or carbon structures with pentagon-incorporated end-edge than pure Ni_{55} cluster.

As depicted in the Fig. 5, the chemical potentials of the carbon Ring5 and Ring6 on the $Ni_{55}C_{20}$ carbides are 1.32 and 1.24 eV (blue round symbol in the Fig. 5), respectively, which are higher than that of all other $Ni_{55}C_n$ carbides. So the saturated nickel carbides may be formed prior to the formation of the carbon rings on them. In addition, the formation of the carbon Ring5 and Ring6 requires a large surface coverage of carbon atoms on the $Ni_{55}C_{20}$ carbide surface because there are high chemical potential barriers at the state of the $Ni_{55}C_{20}$Ring5 and $Ni_{55}C_{20}$Ring6. Subsequently, Fig. 5 shows that the $Ni_{55}C_{20}$Cap20 has lower chemical potential at 0.58 eV, followed by the $Ni_{55}C_{20}$Cap21 at 0.41eV, the $Ni_{55}C_{20}$Cap40 at 0.24 eV, and the $Ni_{55}C_{20}$Cap39 at 0.22 eV, respectively, which are all lower than the $Ni_{55}C_{20}$Ring5 and $Ni_{55}C_{20}$Ring6. So, once the carbon Ring5 and Ring6 form on $Ni_{55}C_{20}$ carbide

surface, they would be spontaneously extended into Cap20 and Cap21carbon intermediates, and then continually grow into complete Cap39 or Cap40 carbon caps.

Beside on the root growth hypothesis, at the initial stage of the SWCNT nucleation, carbon species would first nucleate into chiral caps on the catalyst surface, and then continually grow into corresponding chiral nanotubes. It is generally considered that cap formation process is the critical period in controlling synthesis of SWCNTs. Furthermore, the Carbon caps were uniquely constructed by six pentagons and several hexagons according to the isolated pentagon rule[51, 52], described in details in previous works[26], Therefore, we anticipate high selectivity of metal carbide for the carbon pentagons may play an important role in preferential formation of special carbon caps and SWCNTs. Due to the limitation of computations resources, we explored only two types of typical chiral carbon caps in current work. More extensive calculations are under way in our lab, which includes comparing selectivity behaviors of Ni carbide and pure Ni clusters for various chiral caps and nanotubes

4. Conclusion

We studied a series of $Ni_{55}C_n$ (n=5, 10, 15, and 20) carbides as well as the adsorption of small carbon rings and caps on the $Ni_{55}C_{20}$ in terms of formation energy, adsorption energy and chemical potential. It is found the total energies of $Ni_{55}C_n$ isomers depend on distribution patterns of C atoms among them. Meanwhile, small total energy difference between $Ni_{55}C_n$ (for the same n) implies carbide intermediate

species with different configuration are likely to co-exist in the experimental synthesis. The formation energy of the $Ni_{55}C_n$ carbides has been enhanced gradually with increasing C atomic numbers in nickel carbides, meaning these $Ni_{55}C_n$ carbides are thermodynamically stable. More importantly, the calculated chemical potentials indicate that the $Ni_{55}C_n$ carbides would be preferentially formed, and saturated nickel carbides may be able to exist during initial nucleation and growth process of SWCNTs. Furthermore, the interactions of $Ni_{55}C_{20}$ carbide with carbon rings and caps show that the nickel carbides have a high selectivity for the carbon pentagon and carbon structures with pentagon-incorporated end-edge. These results of the metal carbides strongly correlate to initial nucleation and growth of the carbon caps and SWCNTs. We expect that novel approaches could be developed by engineering metal carbide catalysts by adjusting carbon concentration and distribution pattern, which may further improve control growth of SWCNTs.

Acknowledgments

We acknowledge financial supports by the National Natural Science Foundations of China (21203094, 21373112).

Electronic Supplementary Information (ESI) available: detailed geometric structure parameters for the optimized $Ni_{55}C_n$ carbides (n=5, 10, 15, and 20); Adsorption energy and chemical potential for the carbon rings/caps on $Ni_{55}C_{20}$ carbide and pure Ni_{55} clusters.

References:

1. A. Jorio, G. Dresselhaus, M. S. Dresselhaus and Eds., *Carbon Nanotubes, Advanced Topics in the Synthesis, Structure, Properties and Applications*, Springer, Berlin, 2008.

2. E. Joselevich, H. Dai, J. Liu, K. Hata and A. H. Windle, *Top. Appl. Phys. FIELD Full Journal Title:Topics in Applied Physics*, 2008, **111**, 101-164.
3. J. C. Charlier, X. Blase and S. Roche, *Reviews of Modern Physics*, 2007, **79**, 677-732.
4. X. L. Li, X. M. Tu, S. Zaric, K. Welsher, W. S. Seo, W. Zhao and H. J. Dai, *Journal of the American Chemical Society*, 2007, **129**, 15770-+.
5. H. Kanzow and A. Ding, *Physical Review B*, 1999, **60**, 11180-11186.
6. J. Gavillet, A. Loiseau, C. Journet, F. Willaime, F. Ducastelle and J. C. Charlier, *Physical Review Letters*, 2001, **87**.
7. A. R. Harutyunyan, N. Awasthi, A. Jiang, W. Setyawan, E. Mora, T. Tokune, K. Bolton and S. Curtarolo, *Physical Review Letters*, 2008, **100**.
8. J. C. Charlier, A. DeVita, X. Blase and R. Car, *Science*, 1997, **275**, 646-649.
9. Y. K. Kwon, Y. H. Lee, S. G. Kim and P. Jund, *Physical Review Letters*, 1997, **79**, 2065-2068.
10. A. J. Page, Y. Ohta, Y. Okamoto, S. Irle and K. Morokuma, *Journal of Physical Chemistry C*, 2009, **113**, 20198-20207.
11. S. Irle, Y. Ohta, Y. Okamoto, A. J. Page, Y. Wang and K. Morokuma, *Nano Research*, 2009, **2**, 755-767.
12. S. M. Bachilo, L. Balzano, J. E. Herrera, F. Pompeo, D. E. Resasco and R. B. Weisman, *Journal of the American Chemical Society*, 2003, **125**, 11186-11187.
13. L. Ding, A. Tselev, J. Y. Wang, D. N. Yuan, H. B. Chu, T. P. McNicholas, Y. Li and J. Liu, *Nano Letters*, 2009, **9**, 800-805.
14. D. Ciuparu, Y. Chen, S. Lim, G. L. Haller and L. Pfefferle, *Journal of Physical Chemistry B*, 2004, **108**, 503-507.
15. W. H. Chiang and R. M. Sankaran, *Nat. Mater.*, 2009, **8**, 882-886.
16. M. Lin, J. P. Y. Tan, C. Boothroyd, K. P. Loh, E. S. Tok and Y. L. Foo, *Nano Letters*, 2006, **6**, 449-452.
17. C. Ducati, I. Alexandrou, M. Chhowalla, J. Robertson and G. A. J. Amaratunga, *Journal of Applied Physics*, 2004, **95**, 6387-6391.
18. H. Yoshida, S. Takeda, T. Uchiyama, H. Kohno and Y. Homma, *Nano Letters*, 2008, **8**, 2082-2086.
19. Y. Zhang, Y. Li, W. Kim, D. Wang and H. Dai, *Applied Physics A: Materials Science & Processing*, 2002, **74**, 325-328.

20. S. Hofmann, R. Sharma, C. Ducati, G. Du, C. Mattevi, C. Cepek, M. Cantoro, S. Pisana, A. Parvez, F. Cervantes-Sodi, A. C. Ferrari, R. Dunin-Borkowski, S. Lizzit, L. Petaccia, A. Goldoni and J. Robertson, *Nano Letters*, 2007, **7**, 602-608.
21. A. S. Anisimov, A. G. Nasibulin, H. Jiang, P. Launois, J. Cambedouzou, S. D. Shandakov and E. I. Kauppinen, *Carbon*, 2010, **48**, 380-388.
22. Q. M. Zhang, J. C. Wells, X. G. Gong and Z. Zhang, *Physical Review B*, 2004, **69**, 205413.
23. Y. A. Zhu, Y. C. Dai, D. Chen and W. K. Yuan, *Surface Science*, 2007, **601**, 1319-1325.
24. Y. A. Zhu, X. G. Zhou, D. Chen and W. K. Yuan, *Journal of Physical Chemistry C*, 2007, **111**, 3447-3453.
25. J. Xu and M. Saeys, *Journal of Physical Chemistry C*, 2008, **112**, 9679-9685.
26. Q. Wang, M. F. Ng, S. W. Yang, Y. H. Yang and Y. A. Chen, *Acs Nano*, 2010, **4**, 939-946.
27. F. Ding and K. Bolton, *Nanotechnology*, 2006, **17**, 543-548.
28. A. Borjesson and K. Bolton, *Journal of Physical Chemistry C*, 2010, **114**, 18045-18050.
29. A. J. Page, H. Yamane, Y. Ohta, S. Irle and K. Morokuma, *Journal of the American Chemical Society*, 2010, **132**, 15699-15707.
30. Y. Ohta, Y. Okamoto, A. J. Page, S. Irle and K. Morokuma, *Acs Nano*, 2009, **3**, 3413-3420.
31. A. J. Page, Y. Ohta, S. Irle and K. Morokuma, *Accounts of Chemical Research*, 2010, **43**, 1375-1385.
32. G. Kresse and J. Furthmüller, *Computational Materials Science*, 1996, **6**, 15-50.
33. J. P. Perdew, K. Burke and M. Ernzerhof, *Physical Review Letters*, 1996, **77**, 3865-3868.
34. P. E. Blöchl, *Physical Review B*, 1994, **50**, 17953-17979.
35. G. Kresse and D. Joubert, *Physical Review B*, 1999, **59**, 1758-1775.
36. G. Henkelman, A. Arnaldsson and H. Jónsson, *Computational Materials Science*, 2006, **36**, 354-360.
37. E. Sanville, S. D. Kenny, R. Smith and G. Henkelman, *Journal of Computational Chemistry*, 2007, **28**, 899-908.
38. O. V. Yazyev and A. Pasquarello, *Physical Review Letters*, 2008, **100**, 4.
39. W. M. Zhu, A. Borjesson and K. Bolton, *Carbon*, 2010, **48**, 470-478.

40. A. G. Nasibulin, P. V. Pikhitsa, H. Jiang and E. I. Kauppinen, *Carbon*, 2005, **43**, 2251-2257.
41. Y. Zhang, Y. Li, W. Kim, D. Wang and H. Dai, *Appl. Phys. A-Mater. Sci. Process.*, 2002, **74**, 325-328.
42. Q. A. Wang, K. H. Lim, S. W. Yang, Y. H. Yang and Y. A. Chen, *Theor. Chem. Acc.*, 2011, **128**, 17-24.
43. Q. Wang, S. W. Yang, Y. H. Yang, M. B. Chan-Park and Y. Chen, *J. Phys. Chem. Lett.*, 2011, **2**, 1009-1014.
44. Q. Wang, H. Wang, L. Wei, S. W. Yang and Y. Chen, *The journal of physical chemistry. A*, 2012, **116**, 11709-11717.
45. F. Vines, C. Loschen, F. Illas and K. M. Neyman, *Journal of Catalysis*, 2009, **266**, 59-63.
46. Q. H. Yuan, J. F. Gao, H. B. Shu, J. J. Zhao, X. S. Chen and F. Ding, *Journal of the American Chemical Society*, 2012, **134**, 2970-2975.
47. J. Gao, Q. Yuan, H. Hu, J. Zhao and F. Ding, *Journal of Physical Chemistry C*, 2011, **115**, 17695-17703.
48. A. J. Page, Y. Wang, H.-B. Li, S. Irle and K. Morokuma, *Journal of Physical Chemistry C*, 2013, **117**, 14858-14864.
49. X. Fan, R. Buczko, A. A. Puretzky, D. B. Geohegan, J. Y. Howe, S. T. Pantelides and S. J. Pennycook, *Physical Review Letters*, 2003, **90**, 4.
50. Y. Ohta, Y. Okamoto, S. Irle and K. Morokuma, *Physical Review B*, 2009, **79**.
51. G. Brinkmann, P. W. Fowler, D. E. Manolopoulos and A. H. R. Palser, *Chem. Phys. Lett.*, 1999, **315**, 335-347.
52. S. L. Lair, W. C. Herndon, L. E. Murr and S. A. Quinones, *Carbon*, 2006, **44**, 447-455.